Chapter 11

SHORT NOTES ON PARTICLE IMAGE VELOCIMETRY FOR MICRO/NANO FLUIDIC MEASUREMENTS

C. Y. Lim and Francis E. H. Tay
Institute of Materials Research & Engineering, Singapore

Abstract: Particle image velocimetry (PIV) has emerged as an effective and mature tool for flow visualization and measurement technique for its non-intrusive nature. The basic working principle of a PIV system is deriving the flow velocity from particles' motion in an interrogation window by determining the average displacement within a short period. This approach only yields velocity accuracy up to the first order and inherently assumes that particles travel freely while faithfully following the flow. We briefly discuss the application of PIV in micro/nano fluidic measurements by addressing several important issues, such as the limit of particle size, the limit of diffraction of light, and the instrumentation. Lastly, we include some research directions that we plan to carry out in future.

Key words: particle image velocimetry, micro/nano fluidic measurements, diffraction limit, particle size, epi-fluorescence, CCD camera, fast Fourier transform, cross correlation

1. INTRODUCTION

The ability of making micron-scaled devices integrated with electronic circuits (Micro-Electro-Mechanical Systems, MEMS) frees up plenty of room at the bottom for research. Things are made smaller to achieve better response time, materials/waste saving and cost effectiveness. These devices, including microfluidic components and biotech integrated chips-on-glass, are inherently involved in low-Reynolds-number flows, in which inertial forces are negligible and

viscous and other forces dominate. Some interesting properties of these flows are that turbulence is nonexistent by nature and hence that diffusion plays a vital role in mixing and that the onset of slip of liquid at this reduced dimensions has been reported, bringing much concern about the applicability of the typical no-slip condition at solid wall. Numerical simulations and experimental investigations show change on viscosity in reduced dimensions within molecular scales. These research opportunities lead to a need for a versatile flow visualization and measurement technique that can characterize flow behaviors at submicron or even nanoscales.

Particle image velocimetry (PIV) has emerged as an effective tool for flow visualization and measurement technique for its non-intrusive nature. With a constantly pulsed light source (normally by laser), an image-recording device captures the displacements of particles within short time intervals, allowing the determination of the flow velocity vector field. Two key performance indicators of PIV system are its dynamic velocity range (DVR) and dynamic spatial range (DSR) [1]. DVR of a measurement, or the ratio of maximum measurable velocity to minimum resolvable velocity, is primarily dependent on the interval of two successive images that are produced by the light source; this is also implicitly reliant on the resolution of the recording device. By considering only a smaller time interval, DVR can be improved considerably by having a shorter pulse interval under unchanged experimental conditions, which will ultimately reach the bottleneck due to recording device's frame speed and sensitivity to light. On the other hand, the ability to resolve detectable particle displacement over dimension of interest defines the DSR. As the dimension goes down, detectability of displacement should follow the same scale to keep the dynamic spatial range constant, which is eventually limited by the resolution of the imaging device. We briefly discuss a PIV system tailored for this application in the following section. We then look at some critical concerns that arise in conducting PIV measurements as the dimensions reduce to micro/nano scales, which include arisen issues due to the size of seeding particle and the required instrumentation associated some theoretical background. Lastly, we discuss some potential research interests in related applications.

2. BACKGROUND OF MPIV

A basic PIV system produces particle images with a thin sheet of light often provided by a laser beam and a camera for image recording. These images are then correlated using fast Fourier transform (FFT) and are usually

treated with other post-processing techniques before a good quality measurement can be obtained. Optical microscope is often required for magnifying the tiny region of interest and projecting it to the CCD array. Vibration isolation is essential in singling out environmental noise from Brownian motions of particles.

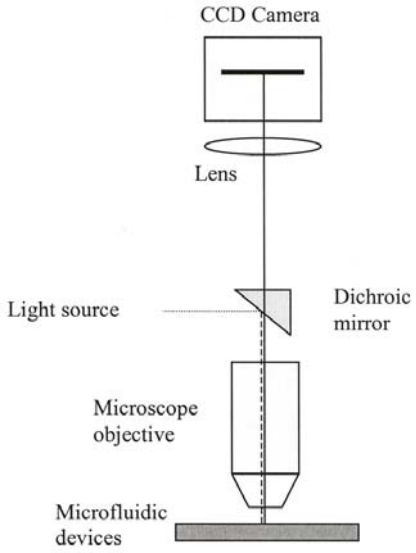

Figure 1. A typical μPIV set up, including the illumination, CCD recording device, a microscope, and microfluidic devices

Good quality images for PIV can be produced by appropriate choice of equipment in system integration. Pulsed lasers gain their popularity as the light source for their ability to deliver thin light sheet with precise duration and interval to freeze particles in motion without using a mechanical shutter. A high-speed high resolution CCD camera is desired to yield micron-order resolution, and an objective nano-positioner to enable focusing on nanometre order. An epi-fluorescence microscope is usually required to zoom in as well as to yield inelastic light scattering for viewing tiny particles (nanometre range). PIV measurements require a synchronized system that integrates all devices, starting from triggering laser pulses for illumination and CCD camera frame grabbing, digital data transfer and storage for offline data analysis. Lastly, the post data processing can be done using mature commercial software, which is essentially an auto- or cross-correlation algorithm locating the peak and deriving the velocities of particles by

statistical means within interrogation windows. Digital approach is preferred and used extensively due to occurrence of high-resolution digital cameras; optical means together with photographic-film camera was widely used in early days in performing correlations for displacement peaks. Figure 1 is a schematic diagram depicting a typical μPIV system.

2.1 Working Principle

The basic working principle of a PIV system is deriving the flow velocity from particles' motion in an interrogation window by determining the displacement Δx within a short period Δt as in the following equation:

$$v = \frac{d\mathbf{x}}{dt} \approx \frac{\Delta \mathbf{x}}{\Delta t} \tag{1}$$

This approach inherently assumes that particles travel freely while faithfully following the flow. Note that due to its simplified nature, the velocity obtained is only accurate up to the first order; no knowledge on curved motion can be retrieved (see Fig. 2). In this case, particle size gives an upper limit below which they will follow the flow faithfully, while Brownian motion and light scattering impose the lower limit on the size suitable for seeding. PIV is in overall a statistical means for measuring flow velocities, i.e. particles within an interrogation window with density N_p yield only one velocity vector. Hence, flow imaging and image capturing are important in conducting experiments to produce accurate and quality results; this is particularly true for micro/nanoflows with extremely small dimensions and velocities. With the above system, resolution (which is the size of the first interrogation window) of order of a micron can be achieved in principle, while further improvement in resolution may be achieved by minor change of hardware as well as innovative design of experiment. Local measurements such as concentration (obtained from different fluorescence levels of dyed particles) and velocity can also be obtained, which can be used to further derive other flow properties such as vorticities, strain rate, Reynolds fluxes, etc.

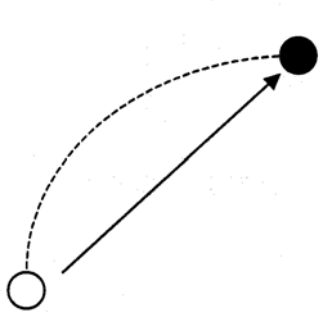

Figure 2. The first order velocity accuracy in PIV system, in which non-linear motion is essentially overcome by having small time interval Δt Auto- and Cross-Correlations

Early PIV [2] used primarily autocorrelation technique in locating displacement peak due to technological availability and historical reasons (particle streaking), which involved essentially doubly exposed images. This effectively increases the image density within an interrogation spot and enhances the correlation peaks. However, not only this method has a narrow range of DVR and hence limited to low-speed measurements, it imposes directional ambiguity for two displacement peaks occur by each side of the self-correlated peak, as shown in Fig. 3(a). Figure 3(b) briefly shows how an auto-correlation can be carried out with a frame of image. Image shifting using a rotating mirror solves the directional ambiguity and broadens the DVR, but further complicates the operations and setting up of the apparatus.

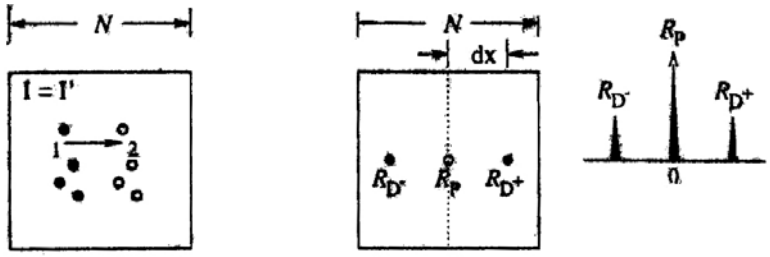

Figure 3(a). Autocorrelation by doubly exposed frames, yielding a strong self-correlation peak and two identical displacement peaks that cause directional ambiguity

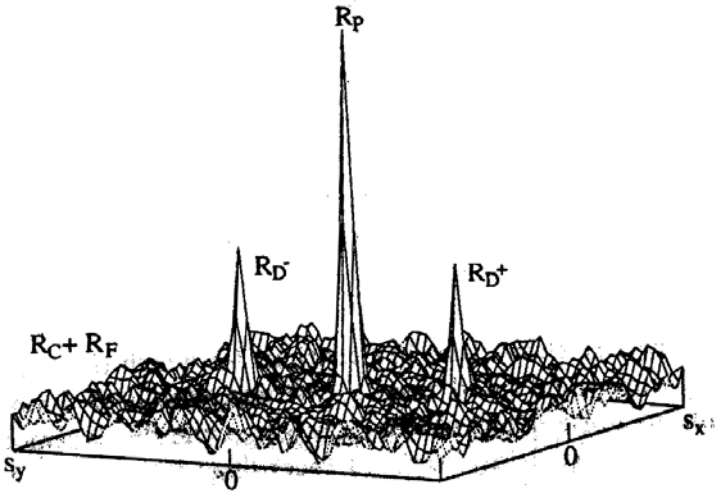

Figure 3(b). Intensity peaks of a self- (R_S) and two displacement-correlations (R_D) in symmetrical arrangement, as well as other much smaller peaks that are composed from convolution R_C and background noise R_F

On the other hand, cross-correlating two consequent images eliminates the directional ambiguity as the sequence of images is known. This approach, often used together with digital cameras, becomes very popular among its practitioners due to its clear directionality and simplicity. Figures 4(a) and 4(b) show how a cross-correlation of two images can be carried out and the resulting peaks after cross-correlation. By the correlation theorem, it can be shown that Fourier transform of the cross-correlation of two functions is equivalent to a complex conjugate multiplication of their individual Fourier transforms:

$$\hat{R}_{II} \Leftrightarrow \hat{I} \cdot \hat{I}'^{*} \tag{2}$$

where R_{II} is the cross-correlation, I and I' intensity values of images and superscript ^ and * denote the Fourier transform and the complex conjugate respectively. Hence, two real-to-complex, two-dimensional (2-D) Fourier transforms plus one complex-to-real, 2-D inverse Fourier transform are needed for each cross-correlation. Figure 5 summarizes the implementation of cross-correlation using Fourier transform and its inverse. In practice, the Fourier transform is efficiently implemented for discrete data using the fast Fourier transform or FFT which reduces the computation from $\boldsymbol{O}(N^2)$ operations to $\boldsymbol{O}(N\log_2 N)$ operations [3]. This effectively reduces the normal

cross-correlation procedure of two two-dimensional images $\boldsymbol{O}(N^4)$ operations to only $\boldsymbol{O}(N^2 log_2 N)$ operations, as shown in Fig. 5.

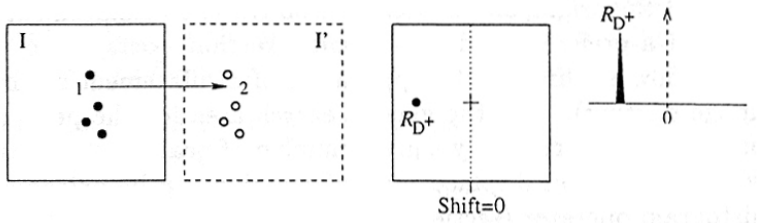

Figure 4(a). Cross-correlation by two different frames, giving only one clear displacement peak eliminating directional ambiguity encountered in auto-correlation

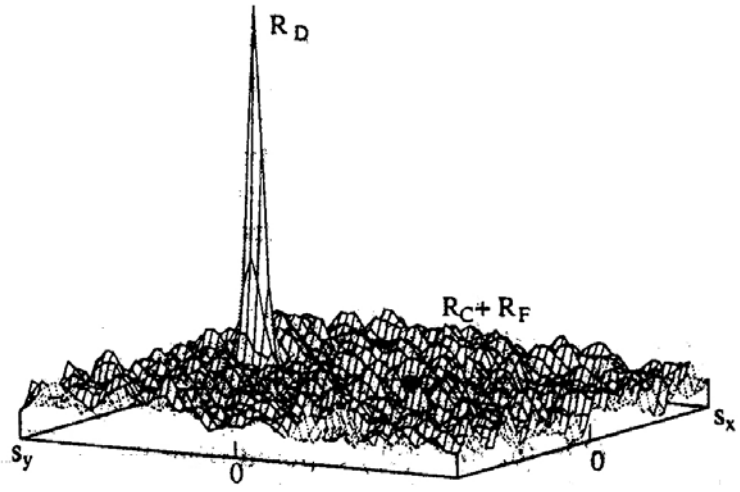

Figure4(b). A typical cross-correlation function, including a strong displacement peak R_S and others due to convolution R_C and background fluctuation R_F

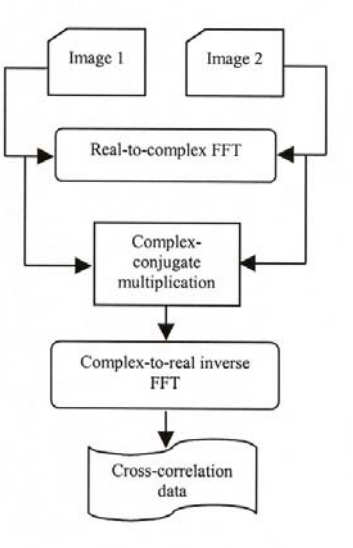

Figure 5. Two 2-D real-to-complex FFT, followed by complex-conjugate multiplication and then a complex-to real inverse FFT in computing a cross-correlation digitally

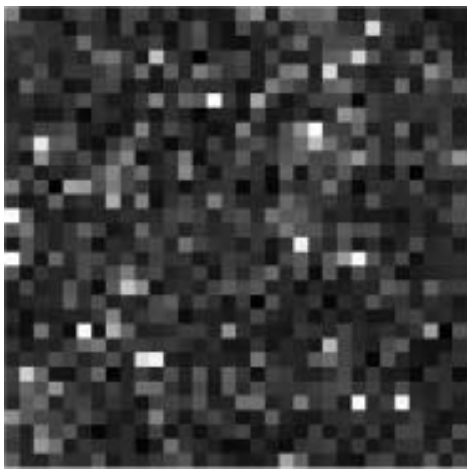

Figure 6(a). A fraction (32X32 pixels) of PIV recording taken in experiments for wake vortex flow behind a transport aircraft, which was originally imaged with digital resolution of 1280X1024 pixels

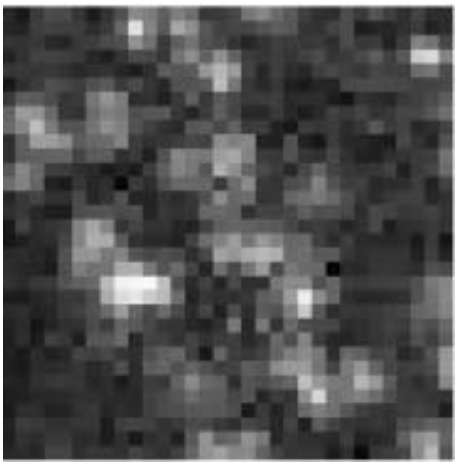

Figure 6(b). A fraction (32X32 pixels) of PIV recording taken in experiments for microchannel flow with digital resolution of 1100X930 pixels

Figures 6(a) and 6(b) give some idea of how those tracer (seeding) particles will appear on a digital CCD image, which are extracted from macroscopic wake vortex flow [4] and micro-channel flow respectively [5]. These particles appear to be squares on a checkerboard rather than of their normal shapes and that they seem to have higher noise ratio for micro-channel flow under high magnification. By presuming that particle images are Gaussian distributions, centroids of particles and therefore their locations can be determined within one tenth of their sizes, which in turn improves the resolution considerably [5].

3. SEEDING PARTICLES

Apart from fabrication of tiny channels with various complex geometries, which is not directly related to the measurement system, the size of the particle stands out as the primary obstacle for tiny length-scale measurements, as the size of those particles must be negligible compared to the area of interest. This is to ensure negligible disturbance of flow by the seeded particles, and to maintain the faithfulness of particles in tracking the flow. Conventional PIV measurements involve mostly particles of 1μm size, which brings in no significant drawbacks discussed above. Sharp [6] reported clogging of microcapillaries by 1μm particles, in which further reduction of the size of laden particles was restricted by their image detectability due to light refraction at round capillary wall.

A corresponding size for the seeding particles used in visualizing microfluidics is often much smaller than the flow dimensions. At these scales, normal elastic scattering of light will not be sufficient in delivering good images. The submicron requirement in seeding particles in modern PIV measurements calls for inelastic light scattering such as fluorescence technique in rendering sufficient intensity of light. Little investigation has been carried out on the direct scale-down of seeding particles. Adrian *et al.* [7] concluded that at least ten particle images were required to yield sufficient signal to noise ratio for good quality cross correlations via Direct Simulation of Monte Carlo (DSMC). Note also bare measurements without additional optical equipment are almost impossible. Modern PIV system often incorporates a microscope when used in measurements of micro/nanofluidics, which only requires minor optical alignment work [8]. In ref. 5 for example, fluorescent particles of size 200 nm were used in 300x30 μm^2 channel, which is a typical example of roughly 150:1 scale-down on seeding particles. More details on the instrumentation will be discussed in the following section.

3.1 Limit of Particle Size

In addition to the direct scale-down of the particle size, we need to consider the constraint of size imposed by the contraction of area of interest in the context of fluid mechanics. Assuming that the particles follow the flow 'faithfully' so that the velocity difference of particle and flow is small compared to the flow velocity, from Newton's second law

$$\left|\vec{v}-\vec{u}\right|\left(\vec{v}-\vec{u}\right)=\left[\frac{2\rho_p d_p}{3\rho C_D}\vec{a}\right] \tag{3}$$

where $\vec{v}$, $\vec{u}$, $\vec{a}$, ρ, and d are respectively particle velocity, flow velocity, particle acceleration, density (flow) and particle diameter, subscript p denotes particle, and the drag coefficient

$$C_D=\frac{24}{\mathrm{Re}} \tag{4}$$

according to Stokes' law for flow past a sphere, $\mathrm{Re}=\vec{u}d_p/\nu$ is the Reynolds number, ν is the kinematic viscosity. Equations (1) and (2) ultimately gives 0.06 μm at condition $\left|\vec{v}-\vec{u}\right|\le 0.0001\left|\vec{u}\right|$ with a time scale of 1μs. This limit renders a guideline when determining size of particle for μPIV measurements, before further consideration of other factors such as

effect of Brownian motion, sufficiency of scattering light, and magnification and diffraction limit.

Brownian motion of particles due to diffusion has to be considered when submicron particles are used. By definition, Brownian motion is the irregular movement which small particles of microscopic size carry out due to osmotic pressure when suspended in a liquid, which defines the root mean square of the diffusion distance Δ [9]:

$$\sqrt{\overline{\Delta^2}} = \sqrt{2D}\sqrt{\tau} \tag{5}$$

where τ is the time scale of diffusion and D is the coefficient of diffusivity, given by

$$D = \frac{kT}{3\pi\eta d_p} \tag{6}$$

in which k is the Boltzmann constant, T is the absolute temperature, η is the coefficient of dynamic viscosity, and d_p is the diameter of suspended particles. Santiago *et al.* [8] estimated the relative error due to Brownian motion by displacement of particle Δx following faithfully the flow with velocity u within time τ ($\Delta x = u\tau$) to be

$$\varepsilon_B = \frac{\sqrt{\overline{\Delta^2}}}{\Delta x} = \frac{1}{u}\sqrt{\frac{2D}{\tau}} \tag{7}$$

In their work, the error was reduced by ensemble averaging, which improves the diffusive uncertainty to $\varepsilon_B/\sqrt{N}$, where N is the total independent samples constituted by eight instantaneous realizations of an interrogation spot with five particle images on average. This ensemble averaging reduces effectively the unbiased Brownian uncertainty, and for the example of N = 40, the error can be improved by more than six times.

3.2 Limit of Light Diffraction

The image of a distant point source through a circular aperture does not appear as a point, but forms a circular diffraction pattern known as Airy disk on the image plane, as illustrated in Fig. 7(a). If the intensity distribution of the point response function of the lens and the light distribution of the particle by objective are approximated by Gaussian functions, then the image

intensity, according to Adrian and Yao [10], will also be Gaussian with the effective diameter given by the following equation:

$$d_e = \sqrt{M^2 d_p^2 + d_s^2} \tag{8}$$

where M is the magnification of lens, d_p is the particle diameter, and d_s is the diameter of point response function of a diffraction-limited lens measured at the first dark ring of the airy disk intensity distribution:

$$d_s = 2.44(M+1) f_{\#} \lambda \tag{9}$$

in which $f_{\#}$ is the focal length divided by the aperture diameter and λ is the wavelength of light. Figure 7(b) shows the close fitting of a Gaussian approximation in representing Airy function for mathematical simplification. Note that if the particle size goes below the wavelength of light, the effective diameter captured will be nominated by the diffraction. Consider a 0.06 μm particle that contributes to only 0.8% of the effective image for 100X and numerical aperture (*N.A.*) of 1.4, which clearly depicts the dominance of diffraction at small diameters. *N.A.* is a direct indication of the ability of lens in gathering light and resolving objects. A direct approximated relationship between numerical aperture and focal number is given as below [11]:

$$NA = \frac{1}{2 f_{\#}} \tag{10}$$

It is clear from the above example that reducing the size of the particle will have insignificant effect on the effective image captured, which in strict sense can only be improved by using better lens (higher *N.A.*) or shorter wavelength of light. Hence, the appropriate size of particle is compromised in between Brownian motion uncertainty and the faithfulness of particle in following the flow from fluid mechanics point of view; also volume occupation of particles within an interrogation spot should be an indication of whether the existence of suspended particles are disturbing the flow. Meinhart *et al.* [5] used 0.05% occupation volume of 200 nm particles for their 13.6X0.9X1.8 μm^3 interrogation window, which was a slightly conservative value compared to conventional flows (0.07% for 1x1x1 mm^3 with 1 μm particles).

Figure 7(a). A typical Airy disk from light passing through small circular aperture

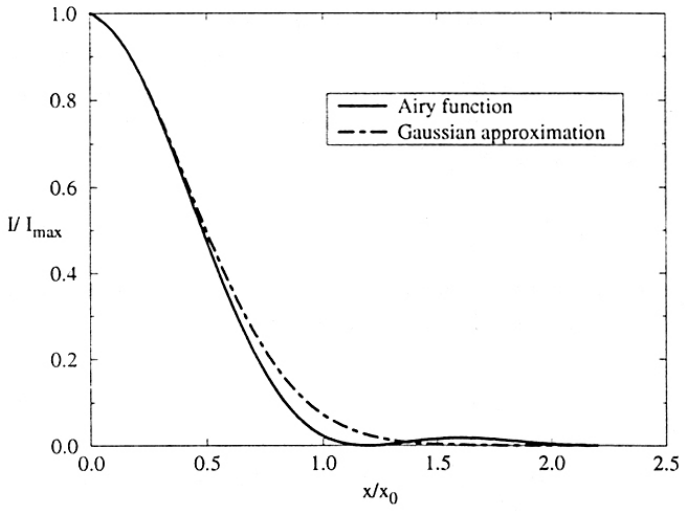

Figure 7(b). A fitting of Gaussian function to approximate Airy function, which simplify extensively mathematical equations involved in optics theory

4. INSTRUMENTATION

Tiny particles in submicron range often have the problem of yielding adequate scattered light for image capturing, as the scattering power is proportional to the fourth power of their diameters [12]. Together with optical and technological limitations on instrumentations, the size of the particle suitable for μPIV applications is confined to a narrow notch, within which yields sufficient light for their images to be captured (often by a CCD camera) while tracking the flow faithfully in strict sense of fluid mechanics. Fluorescent particles are becoming a popular alternative solution as they fluoresce instead of having light scattered elastically ($\propto d_p^4$). This inelastic

scattering of light requires an excitation ray of certain range of wavelength in order to emit light of longer wavelength (Stokes' shift). With diameters of 300 nm or less (below visible light wavelength), the light intensity is still very limited by the size; relatively strong pulse of laser is required to achieve acceptable intensity that is good enough for image capturing and processing. This imposes another problem, as the light reflected by the background surfaces often acts as high background noise that will deteriorate the signal to noise ratio of particle images. In the following sections, we briefly describe the instrumentation used in modern flow visualization system for miniaturization, which consist of an image recording system, an optical microscope, and delivery systems.

4.1 Image Recording

The basic working principle of PIV lies on recording images of particle displacements, which show the fluidic motion within interrogation spots after performing data processing. As a result, good quality images are therefore essential for high quality measurements. Photographic films are preferred for its much higher spatial resolution compared to CCD sensors, and are frequently used in turbulence and other measurements featuring high velocity and spatial resolution. However, photographic film technique often has a disadvantage in data processing as analogue data need to be converted to digital data manually for auto or cross correlations using a computer. On the other hand, CCD sensors convert photons received into electric signals, and these digitised data can be fed directly to a computer for further processing. Note that CCD array is strictly an analogue device by itself, but the associated technology in transfer and storage and its heavy dependence on computer make it a digital device. As high-resolution CCD cameras are commercially available at affordable prices now, CCD cameras are becoming very popular in modern PIV measurements. As the scarcity of light is the major factor in getting good images of particles for μPIV application, the CCD array is normally nitrogen or air-cooled to eliminate dark current due to thermal effect. Large dynamic range of a CCD array is also preferred, i.e. a 12 bit range will have 4096 grey levels in resolving background noise and real signals. It carries 16 times more information than that of an 8 bit range by providing higher resolution on the grey levels and therefore is more beneficial in quantitative analysis. In addition, an elegant alternative is to employ an epi-fluorescence microscope, which is discussed in the following section. Another way to improve the signal to noise ratio is through binning, in which several adjacent pixels are combined during readout to yield greater signal. A 2X2 binning will improve four times the signal to noise ratio by providing four times more electron with constant

read noise while shrinking four times the measurement area. A side advantage of binning is to increase the frame rate with the reduction of number of pixels to be readout.

The size of a single CCD pixel, which is also the smallest resolvable length in terms of instrumentation, has an important role in defining the DVR and DSR of the device for arbitrary flow measurements, which in turn limits the maximum flow velocity and physical area of interest. However, the image of an effective particle projected on CCD sensors is usually an order larger than a pixel size, this makes the pixel size not a premium consideration factor in improving experimental resolution. Take our previous particle for instance, the effective diameter under 100X with *N.A*=1.4 is roughly 50 μm, while a typical CCD pixel size is about 6~7 μm. In this case, about ten pixels are required for an image of a particle; this implies that further refining the size of pixel does not improve the resolution effectively. On the other hand, since the flow area is zoomed in under magnifications, larger array of CCD sensors gives more allowance on the physical area of interest, or better resolution (in terms of vector counts) with the same physical area provided the particle size is larger than 3~4 pixels [13]. The spatial resolution is usually defined as the first interrogation window of the image, which is often associated with an optimum seeding density. Depending on experiments, optimum number of particles within an interrogation window ranges from 5 to 20. With larger array of CCD sensors, the measurement resolution can be increased accordingly because either the flow domain can be better resolved spatially with more pixels within the same size of interrogation window or the flow field being measured can be extended with respect to the increase of CCD sensors. Larger array of CCD sensors also tends to have less error in capturing and locating particle images that fall in between sensors. A projected image on CCD with 13μm (corresponding to a minimum of 2 pixels in resolving an particle image) forms the lower limit of which tracer particle size can be reduced taking into consideration of magnification and diffraction.

Normal CCD camera that has a 30 frames per second can be used in conjunction with the frame straddling technique, which arranges two closely delayed laser pulses at the change of two successive frames (frame straddling) [14], as illustrated in Fig. 8. Two back-to-back images can be obtained within 200 ns with current CCD camera's technology, which is sufficient to cover almost all the velocity range in fluidic measurements. Such a high temporal resolution is impracticable with a continuous wave laser and a mechanical shutter economically. While short temporal delay of laser pulses is desired to improve correlation peak intensities by eliminating the out of plane movements and in-plane losses (loss of particles within two

correlation windows), it is a rigid parameter whose change is associated with other factors such as the fluid velocity, optical magnification, and interrogation window. Note also that time resolved studies are impossible using this technique.

We mentioned earlier that background reflection constitutes a huge portion of noise, and suggested that a cooled, high dynamic range CCD camera to be used. A direct quick means is to place a filter in front of the CCD camera that will block out the excitation light reflected by the background. We will look at another way to overcome this problem, taking advantage of the Stokes' shift of the fluorescence in the following section. We devote a paragraph of basic quantum physics to depict what Rayleigh (elastic) scattering, Raman scattering, fluorescence (inelastic scattering), and phosphorescence are in the following.

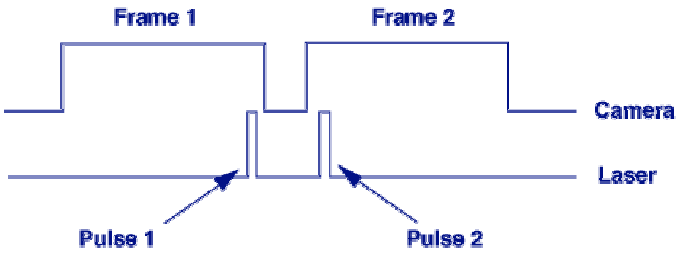

Figure 8. Frame straddling used in PIV measurements to provide a much faster frame rate where two laser pulses are shot at the changing of frames. Note that these pictures taken back-to-back cannot render time-resolved behaviors at the rated frame rate

Rayleigh scattering is the absorption and re-radiation of light by an object, which does not involve electron transition and energy loss, and therefore causes no shift in wavelength. When a molecule in the base state S_0 is exposed to light (energy higher than the threshold), the kinetic energy of the electrons in the molecule is increased, shifting the molecule into the excited state S_1 with a higher energy level as shown in Fig. 9(a). The excited molecule is unstable, so the high-energy electrons will undergo some radiation-less transition to a lower excited state within a short period of time, from which they go back to the base state radiating the excessive energy in the form of light. This is called a Stokes' shift. The associated energy loss during the radiation-less transition is dissipated via vibration and heat, and the emission after Stokes shift therefore has lower frequency/longer wavelength than that of the excitation in accordance to the energy equation:

$$E = hf = \frac{hc}{\lambda} \tag{11}$$

where E is energy of emission, h is Planck's constant 6.626×10^{-34} Js, c is the speed of light, and λ is the wavelength of radiation. Further radiation-less transition to lower energy level leads to phosphorescence, which has longer life span than fluorescence. Figure 9(b) shows the excitation and emission spectra of 0.06μm dyed-polystyrene beads in DI water with 2% solid, where a 30nm Stokes' shift was reported. Note that the sharp excitation spike in the emission spectrum that is caused by Rayleigh scattering of suspended particles.

4.2 Epi-Fluorescence Microscopy

A typical epi-fluorescence microscope comprises a filter cube capable of allowing only the emission of the fluorescence from the particles to pass through the barrier filter and at the same time reflecting any other rays having shorter wavelength by a dichroic mirror. Inverted microscope has recently been used for this purpose in microchannel measurements [5], together with a pulsed Nd:YAG laser system capable of delivering 5 ns pulses with 500 ns delay. The additional component that a μPIV system requires compared to its macroscopic counterpart is essentially the microscope. By incorporating the epi-fluorescence function to the microscope, not only it helps magnify the test section to the desired size, it plays a vital role in coordinating the excitation and emission light to yield high signal to noise ratio in recorded images.

Volume illumination rather than sheet illumination is applied in microfluidic measurements because of the difficulty in delivering a comparatively thin laser sheet corresponding to the flow measurement area. For instance, a typical micro-channel measurement requires 1~10μm laser sheet properly aligned to the area of interest for a typical out of plane resolution of similar scale, and this is of great difficulty if not impossible in both producing and aligning such a thin sheet of laser, and only volume illumination remains practical [15]. As a result, the out of plane resolution is defined by the measurement depth of the system. The measurement depth is twice the distance from centre of the object plane at which a particle can be located such that its maximum image intensity is an arbitrarily specified fraction of its maximum in-focus intensity, beyond which the particle image intensity will only be perceived as noise.

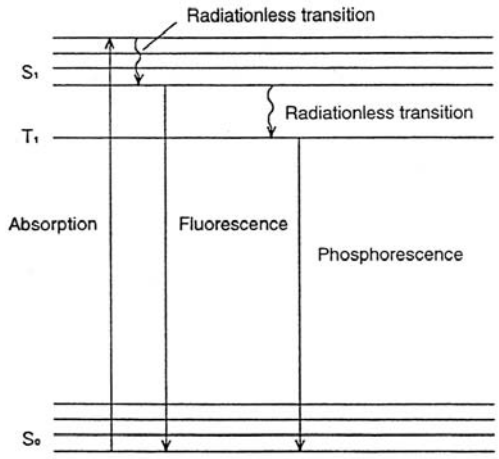

Figure 9(a). The principle of fluorescent emission involving absorption and conversion of photon energy into electron energy, in which energy loss due to vibration and heat imposes a shift of energy into longer wavelength

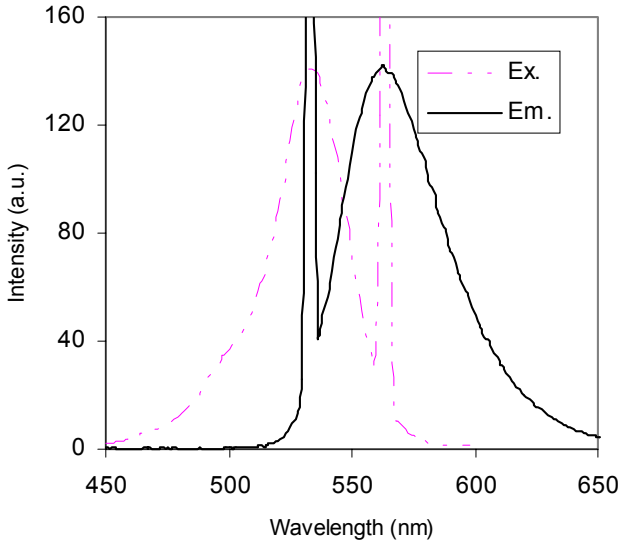

Figure 9(b). Excitation and emission spectra of *Bangs Labs Inc.*'s 0.06μm dyed polystyrene microbeads captured using *Shimadzu*'s RF-5301PC spectrophotometer, in which the Rayleigh scattering of suspended particles are clearly shown in both spectra

4.3 Delivery Systems

Delivering liquid flow at desired experimental conditions is a mandatory procedure for any microfluidic experiment to be carried out. Precision syringe pumps have been popular in delivering constant flow rate of typically 200 μl/hr [5]. A 'blow-down' of a highly charged pressure vessel provides consistent flows for a considerable period as the pressure deteriorates, which generates high velocity of flow for high Re applications [6]. Another approach worth mentioning is the electrokinetically driven flow by Paul *et al*. [16], which produces plug-like flow profile by applying a high-voltage dc electric field along the capillary between platinum electrodes. Other innovative practices include vertical adjustment of manometers' positions that are connected to ends of microchannels and by gravity (slanting the microchannel).

The microchannel may be fabricated from silicon wafer, etched from glass, or even off-the-shelf flexible fused silica capillaries, depending upon the research motives. Take the capillary tubing that is commercially available for example: the tiny tubing is usually coated with polyimide for protection, and ferrules are used at ends to enhance better grip between the tubing and other adapters connecting to conventional tubes (1/8 or ¼ inch in diameter). In the case of a larger interaction area, such as a mixing field for micromixer, only glass etching and anodic bonding can be feasible at laboratory scale. Nanoports that can be adhered on glass by *Upchurch Scientific* provide reliable fluid connections for lab-on-a chip devices.

5. POTENTIAL INTERESTS OF RESEARCH

The research opportunities are many-folded with this enabling instrumentation. The slip and viscosity measurements can be obtained directly from the velocity field obtained by PIV, in contrast to effort found in the literature that mainly concentrate on measurement of flow rate for slip investigation and measurement of the induced force by SFA (Surface Force Apparatus) for viscosity derivation. Whole-field visualization of a mixing junction [17] yields a better insight of fluidic interaction and vortices formation at low Reynolds number. Another interesting phenomenon under this low Reynolds number condition is the mixing of two fluids by merely diffusion, which is insignificant compared to that induced by turbulence at macroscopic dimensions. An investigation on diffusion of particles within two fluids through a

mixing channel has been reported in the literature [18]. The ability in visualizing fluidic flow in reduced dimensions renders better understanding in fundamentals in micro/nano fluid dynamics. Fundamental fluid dynamics at submicron scales can be better understood by carrying out field measurements over obstructing objects and over complex geometries. We briefly discuss some research areas that we identify as interesting research scopes below.

5.1 Miniaturization Effects

At much reduced length scales, it is generally agreed that the static properties of fluid will remain unchanged. However, increasing interests have been focused on the dynamic properties, such as the dynamic viscosity of the fluid. Pfahler *et al.* [19] reported a decrease in apparent viscosity by measuring the flow rate without considering slip effect, while other groups concluded an increased apparent viscosity while losing fluidity (becoming solid-like) at monolayers above the wall by surface force apparatus (SFA) [20]. An associated phenomenon in this reduced length scale is the onset of slip. Bocquet and Barrat [21] reported no slip above ten monolayers, while Churaev *et al.* [22] discovered remarkable slippage of liquids over lyophobic solid surfaces. Here we propose to study both viscosity and slip of liquid at small dimensions, looking at the facts that both of them are related to shear on surfaces and that both are constituted by velocity, of which our proposed PIV system is capable of measuring.

5.2 Fundamentals and Fluid Dynamics

Fundamentals of fluid dynamics for micro/nano scales can be studied using the proposed PIV system, which renders a direct flow measurements compared to other indirect measurements, such as shear force, bulk flow rates, etc:

- Flow past an electrically/magnetically held still μsphere – a particle is to be held still electrically/magnetically in a microchannel against a stream of fluid flowing past; where we intend to study Stokes' law and Navier-Stokes equation for submicron spheres.
- Two dimensional micro/nanofluidics – visualizing flow past a circular cylinder matrix in Hele-Shaw cell at submicron level can be meaningful in studying wake and vortex formation in the strong presence of viscosity.
- Vortex formation in low-Reynolds-number flows – turbulence is inherently non-existent for $Re << 1$ as any perturbation will be damped out by the dominating viscous force; however, Brody [23]

reported vortex formation near an air/fluid interface. We intend to study these interfaces by forcing a bubble through a microchannel; the vortices formed may be a good source for mixing in low-Reynolds-number flow.

5.3 Other Potential Research Opportunities

With this PIV system, characterizations of microfluidic devices can also be done. For example, a crossed junction can be fabricated to characterize the hydrodynamic focusing of main flow by 2 side flows [17]; diffusion of fluorescent particles to a buffer can be investigated along a mixing microchannel by combining velocity and concentration measurements; in both cases fluid dynamics can be studied at submicron scales, which may eventually decrease down to nano scales. The *in situ* hydrodynamics in a carbon nanotube can now be studied, in which movement of bubble in a 100 nm nanotube was reported [24]. This will be the benchmark of our ultimate goal of achieving a nanoscale PIV system.

6. CONCLUDING REMARKS

PIV is a mature technique for macroscopic flow measurements since 1980s. Extending its application to micro/nanoscales is straightforward if a few issues are well taken care of. These include primarily finding a suitable size of fluorescent particles according to optics theories and fluid mechanics, and secondarily, integrating proper instrumentations to yield good quality images within desired range of velocity and spatial resolution for post-data processing. Subsequently, several methods in providing wide range of flow velocities are identified and discussed. We infer that μPIV will serve as an enabling tool in modern flow visualization and measurement technique in the foundational and developmental exploration in this miniaturization era. Its enhanced features extend current research capabilities and provide more flexibility in maneuvering experiments. This provides a better insight of fluid dynamics at reduced dimensions, and makes itself an essential tool in characterizing and helping in design of microfluidic in addition to the viscosity deviation and slip onset. In particular, studies on flow past a nanosphere and micro/nanofluidics under electric and magnetic fields are also made possible. While μPIV remains an enabling equipment for

micro/nanosystems, it serves as a stepping-stone in designing other enabling instrumentations which would better complement micro/nanosystems by understanding the prerequisites in characterizing micro/nanofluidic behaviors and measurements.

REFERENCES

[1] R. J. Adrian, "Dynamic ranges of velocity and spatial resolution of particle image velocimetry," Measurement Sci. Tech., Vol. **8**, 1393 (1997).

[2] R. J. Adrian, T. Asanuma, D. F. G. Durao, F. Durst, J. H. Whitelaw, "Laser anemometry in fluid mechanics-III, Selected papers from the Third international symposium on applications of laser anemometry of fluid mechanics," Ladoan, Lisbon, Portugal (1988).

[3] E. O. Brigham, *The fast Fourier transform* (Prentice-Hall, New Jersey, 1974).

[4] J. Kompenhans, L. Dieterle, H. Vollmers, R. Stuff, G. Schneider, T. Dewhirst, M. Raffel, C. Kähler, J. C. Monnier, K. Pengel, "Aircraft wake vortex investigations by means of particle image velocimetry" measurement technique and analysis methods," In Proceedings of 3rd International Workshop on PIV, Santa Barbara, USA (1999).

[5] C. D. Meinhart, S. T. Wereley, J. G. Santiago, "PIV measurements of a microchannel flow," Experiments fluids, Vol. **27**, 414 (1999).

[6] K. V. Sharp, "Experimental investigation of liquid and particle-laden flows in microtubes," Ph. D. Thesis, University of Illinois at Urbana-Champaign (2001).

[7] R. D. Keane and R. J. Adrian, "Theory of cross-correlation analysis of PIV images," Appl. Scientific Res., Vol. **49**, 191-215 (1992).

[8] J. G. Santiago, S. T. Wereley, C. D. Meinhart, D. J. Beebe, R. J. Adrian, "A particle image velocimetry system for microfluidics," Experiments Fluids, Vol. **25**, 316 (1998).

[9] A. Einstein, *The Brownian Movement* (Methuen & Co., London, 1926).

[10] R. J. Adrian and C. S. Yao, "Development of pulsed laser velocimetry for measurement of fluid flow," in Proceedings, 8th Biennial Symposium on Turbulence, G. Patterson and J. L. Zakin, Eds., 170-186 (1984).

[11] M. Born and E. Wolf, *Principles of optics* (Pergamon Press, Oxford, 1991).

[12] R. J. Adrian and C. S. Yao, "Pulsed laser technique application to liquid and gaseous flows and the scattering power of seed materials," Appl. Optics, Vol. **24**, 44 (1985).

[13] A. K. Prasad, R. J. Adrian, C. C. Landreth, P. W. Offutt, "Effect of resolution on the speed and accuracy of particle image velocimetry interrogation," Experiments Fluids, Vol. **13**, 105 (1992).

[14] M. Raffel, C. Willert, J. Kompenhans, *Particle Image Velocimetry: A Practical Guide* (Sringer, Berlin, 1998).

[15] C. D. Meinhart, S. T. Wereley, M. H. B. Gray, "Volume illumination for two-dimensional particle image velocimetry," Measurement Sci. Tech., Vol. **11**, 809 (2000).

[16] P. H. Paul, M. G. Garguilo, D. J. Rakestraw, "Imaging of pressure- and electrokinetically driven flows through open capillaries," Anal. Chem., Vol. **70**, 2459 (1998).

[17] J. B. Knight, A. Vishwanath, J. P. Brody, R. H. Austin, "Hydrodynamic Focusing on a Silicon Chip: Mixing Nanoliters in Microseconds," Phys. Rev. Lett., Vol. **80**, 3863 (1998).

[18] J. P. Brody and P. Yager, "Diffusion-Based Extraction in a Microfabricated Device," Sensors Actuators, Vol. **58**, 13 (1997).

[19] J. Pfahler, J. Harley, H. Bau, "Gas and Liquid Flow in Small Channels," Micromechanical Sensors, Actuators, and Systems, ASME DSC Vol. **32**, 49 (1991).
[20] J. Van Alsten and S. Granick, "Molecular Tribometry of Ultrathin Liquid Flims," Phys. Rev. Lett., Vol. **61**, 2570 (1988).
[21] L. Bocquet and J.-L. Barrat, "Hydrodynamic Boundary Conditions and Correlation Functions of Confined Fluids," Phys. Rev. Lett., Vol. **70**, 2726 (1993).
[22] N. V. Churaev, V. D. Sobolev, A. N. Somov, "Slippage of Liquids over Lyophobic Solid Surfaces," Journal of Colloid and Interface Science," Vol. **97**, 574 (1984).
[23] J. P. Brody, "Fluid and Cell Transport through a Microfabricated Flow Chamber," Ph. D. Thesis, Princeton University (1994).
[24] Y. Gogotsi, J. A. Libera, A. G. Yazicioglu, and C. M. Megaridis, "*In-situ* Fluid Experiments in Carbon Nanotubes," Materials Research Society Symposium Proceedings, Vol. **633**, A7.4.1-6 (2001).

INDEX